Accepted Manuscript

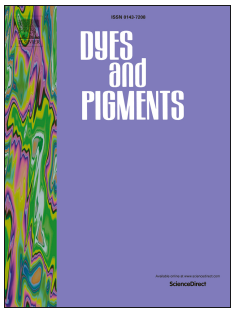

Ratiometric sensing of nerve agent mimic DCP through in situ benzisoxazole formation

Syed Samim Ali, Ankita Gangopadhyay, Ajoy Kumar Pramanik, Uday Narayan Guria, Sandip Kumar Samanta, Ajit Kumar Mahapatra

PII: S0143-7208(19)30143-3

DOI: https://doi.org/10.1016/j.dyepig.2019.107585

Article Number: 107585

Reference: DYPI 107585

To appear in: *Dyes and Pigments*

Received Date: 18 January 2019

Revised Date: 14 February 2019

Accepted Date: 24 May 2019

Please cite this article as: Ali SS, Gangopadhyay A, Pramanik AK, Guria UN, Samanta SK, Mahapatra AK, Ratiometric sensing of nerve agent mimic DCP through in situ benzisoxazole formation, *Dyes and Pigments* (2019), doi: https://doi.org/10.1016/j.dyepig.2019.107585.

Graphical Abstract

Ratiometric sensing of nerve agent mimic DCP through in situ Benzisoxazole formation

Syed Samim Ali,[a] Ankita Gangopadhyay,[a] Ajoy Kumar Pramanik,[a] Uday Narayan Guria,[a] Sandip Kumar Samanta[a] and Ajit Kumar Mahapatra[*a]

[a]Department of Chemistry, Indian Institute of Engineering Science and Technology, Shibpur, Howrah – 711103, India.

*Corresponding author: Tel.: +91 33 2668 4561; fax: +91 33 26684564;

E-mail: mahapatra574@gmail.com, akmahapatra@rediffmail.com

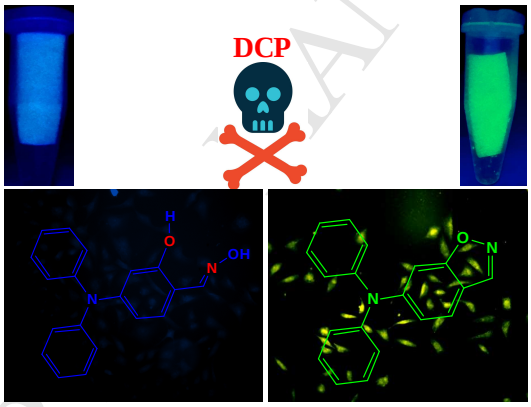

Ratiometric sensing of nerve agent mimic DCP through in situ Benzisoxazole formation

Syed Samim Ali, [a] Ankita Gangopadhyay, [a] Ajoy Kumar Pramanik,[a] Uday Narayan Guria,[a] Sandip Kumar Samanta [a] and Ajit Kumar Mahapatra[*a]

Received (in XXX, XXX) Xth XXXXXXXXX 20XX, Accepted Xth XXXXXXXXX 20XX
DOI: 10.1039/b000000x

Keywords: Ratiometric probe; chemical warfare agents; vapor phase detection in filter paper strip; detection of DCP in soil sample; DFT/TDDFT calculations; cellular imaging; crystal structure analysis.

Abstract

In recent year syria rejuvenate interest in chemical warfare agents (CWAs) for terrorist attacks. Nerve agents are the most scandalous chemicals and can cause death of a person owing to the inhibition of acetyl cholinesterase activity. In this article, we report a colorometric and ratiometric fluorescent probe 4-diphenylamino-2-hydroxy benzaldehyde oxime (**TPOD**) that could be efficient of instant and real-time recording of DCP vapour. Upon reaction with DCP, bathochromic shift from ~463 to ~532 nm was observed due to the inhibition of PET from oxime-hydroxyl to the triphenyl amine moiety and cyclization to the benzisoxazole. The transformation from oxime to benzisoxazole was confirmed by NMR and HRMS data. The probe **TPOD** can be applied on a portable and cost effective test kits where in presence of DCP vapor dramatic color and fluorescence change were observed within 30 secs. Furthermore, the probe can efficiently detect DCP in presence of other nerve agents and electrophile and the detection limit is 0.14 µM. Moreover to evaluate the sensing mechanism we have prepared a control compound **TPD** whose crystal structure and non covalent interactions have been incorporated. To achieve the on-site application of **TPOD** we have performed an experiment in soil sample to detect trace amount of DCP. Moreover the probe can be useful in cellular imaging of DCP containing bio-samples. Thus the probe **TPOD** is an auspicious, instant and on site monitoring ratiometric fluorescent probe for selective DCP detection in presence of other interfering nerve agents.

1. Introduction

Organophosphorous compounds (OPs) include agricultural pesticides, herbicides and chemical warfare agents (CWA) i.e; nerve agents and are regarded as being the most poisonous chemicals to living things ever discovered or synthesized [1-3]. However, the substantial use of these compounds in agricultural industry around the world has generated the poisoning of thousands of humans. In 1936, during synthesis of pesticides, the first nerve agent (Tabun, GA) was

discovered as a by-product [4-6]. OPs, such as sarin, soman, and tabun have also been utilized as nerve agents in chemical warfare [7-8]. So, the potential exposure to chemical warfare agents (CWAs) due to terrorist and military activity has thus become a serious threat to our soldiers and civilians [9-12]. It is evident that the primary toxicity of nerve agents comes from the inhibition of acetylcholine esterases (AChE) by reaction with reactive phosphate group of OPs with the hydroxyl groups of AChE, that prevents the decomposition of acetylcholine. As a result, rapid death of a human, paralysis of central nervous system and organ failure may occur [13,14]. Therefore, a reliable, facile and selective methods are required to resolve the problem. Various sensing methods for nerve agents have been reported [15-17], such as mass spectroscopy/gas chromatography [18-21], electrochemical sensor [22,23], enzymatic sensor [24-26], and interferometry [27-29]. However, these methods have some limitations, such as limited selectivity, low sensitivity, slow response, lack of specificity, operational complexity, non-portability, costly and inconvenient for real-time detection and monitoring [30-32]. So, it is highly appealing to develop a probe which can show distinct changes both in color and fluorescence in the presence of OPs. In this direction, fluorescent chemosensors have attracted significant attention owing to their portability, low cost, highly sensitivity, and easy operation in recent years [33-35]. Generally, diethylchlorophosphate (DCP) is claimed as a nerve-agent mimic owing to its low toxicity but similar reactivity of NAs and hence, a cheap and easy method is most desired for DCP detection.

In this article, we report a new ratiometric chemosensor based on an o-hydroxyl substituted triphenylaminoaldehyde oxime group that can detect nerve agent simulant diethyl chlorophosphate (DCP) very rapidly and selectively in aqueous acetonitrile solution. It comes to light that by deprotonation of an oxime, supernucleophile oximate is formed and is capable of attacking the strong electrophilic organophosphates and accordingly it has been incorporated into sensor system to detect nerve agents [36, 37]. In addition, the oxime group is a well-known medical antidotal treatment for nerve agent exposure [38-41] because “supernucleophile” oxime is capable to restore the serine–OH from the phosphorylated serine–OH in AChE by the attacking at internal phosphorus (serine-O-*P* to serine-OH), and thus the function of AChE reactivates [42-47]. Besides, the o-hydroxy group of the chemosensor enhance the rate of cyclization to generates the benzisoxazole product with a greatly increased sensitivity [48-51]. Moreover, for sensing a target analyte a ratiometric method offers an alternative approach to overcome the disadvantage of intensity based calculations by integrated correction of two emission bands. Finally, ratiometric probe can be employed to detect liquid and gaseous nerve agents [52-55]. Hence, we obtained a concise colorimetric and ratiometric fluorescent probe, bearing an electron donating amine group and rate enhancing o-hydroxyl functionality in the structure, that could realize fast response and is capable of real-time and onsite recording of DCP vapor. A naked-eye detection limit down to 0.14 μM level is remarkably achieved, which makes it a highly optimistic fluorescent sensor for a simple, rapid and low-cost detection for DCP . We have reported another derivative (**TPD**) which is devoid of the ortho-hydroxyl group. In this molecule the characteristic spectrophotometric properties was observed but upon interaction with

DCP appreciable change in absorbance and fluorescence were not observed to the same extent. This proves the participation of ortho-OH in the chemodosimetric reaction mechanism. However the compound **TPD** has been treated as a control compound whose crystal structure (Fig.8) and analytical data (ESI†) have been recorded.

2. Experimental Section

2.1. Chemicals and physical quantification

All the chemicals were obtained from sigma-aldrich and were used without further purification. For NMR spectra, TMS was used as an internal standard and DMSO-d_6 as solvent. ^{1}H and ^{13}C NMR spectra were measured on a Brucker 400 MHz instrument. Chemical shifts and ^{1}H–^{1}H and ^{1}H–C coupling constants are expressed in δ ppm and in Hz units. Mass spectra and fluorescence spectra were done on a Waters QTOF Micro YA 263 mass spectrometer and Perkin Elmer Model LS 55 spectrophotometer.

2.2. Structure optimization study

All calculations for density functional theory (DFT) and Time-dependent density functional theory have been performed using Gaussian 09 program. Optimization of structures have been done using the B3LYP/6-31G (d, p) level of theory. TDDFT calculation has also been carried out at the same level.

2.3. Calculation of detection limit

The detection limit of **TPOD** was calculated on the basis of absorption and fluorescence titration. The absorption and fluorescence spectrum of **TPOD** was measured 10 times, and to get the slope, the ratio of the absorption and fluorescence intensity at 405 nm and 532 nm were plotted as a concentration of DCP. Detection limit was calculated from following equation: Detection limit =3Sb1/S where S is the slope of the calibration curve and Sbl is the standard deviation of the blank measurement.

2.4. Method of solution preparation for UV−Vis titration

Stock solution of **TPOD** and **TPD** (0.4 μM) was prepared in CH_3CN/H_2O (1:1v/ v). All experiments were performed in CH_3CN/H_2O solution (CH_3CN/H_2O = 4:6 v/v, 10 mM HEPES buffer, pH = 7.4). During titration each time 2 ml solution of **TPOD** (8 μM) was charged in a quartz optical cell (optical path length= 1 cm). By using a micropipette slowly the stock solutions of analyte (8 μM) were put in the quartz optical cell.

2.5. Method of solution preparation for fluorescence titration

Stock solution of **TPOD** and **TPD** (0.4 μM) was prepared in CH_3CN/H_2O (4:6 v/ v). All experiments were performed in CH_3CN/H_2O solution (CH_3CN/H_2O = 4:6 v/v, 10 mM HEPES

buffer, pH = 7.4). During titration each time 2 ml solution of **TPOD** (8 µM) was charged in a quartz optical cell (optical path length= 1 cm). By using a micropipette slowly the stock solutions of analyte (8 µM) were put in the quartz optical cell.

2.6. Synthetic procedures

2.6.1. Preparation of compound 1

Phosphorous Oxychloride ($POCl_3$) (3 ml) and DMF (3 ml) were placed in a two neck round bottomed flask, Then the flask was dipped in an ice bath, the stirrer was started, and 3-methoxytriphenylamine (500 mg, 1.81 mmol) dissolved in DMF (1 ml), was added to the $POCl_3$ and DMF mixtures over a period of eight minutes. After completing the addition the mixture was again stirred for 15 minutes. Then the ice bath was separated and again the mixture was allowed to heat at 55-60°C for 6 hr., cooled to the room temperature and poured into ice water. The aqueous part was extricated four times with ethyl acetate. Then organic layer was collected in a beaker and dried over sodium sulfate. Organic solvents were removed in rotary evaporator under reduced pressure. Finally the residue was purified by column chromatography using ethyl acetate in hexane (10% v/v) to give pure 3-methoxytriphenylaminoaldehyde. Light yellow solid, (320 mg, 58.3%), mp: 150-160°C, MS (LCMS): (m/z, %): 321.2 [(**Compound 1**+H_2O), 100 %]; Calculated for $C_{20}H_{17}NO_2$: 303.12. ^{1}H-NMR (DMSO-d6, 400 MHz): δ (ppm) 10.01 (s, 1H), 7.47 (d, J = 8.4 Hz, 1H,), 7.32 (t, 4H), 7.05 (m, 6H), 6.96 (s, 1H), 3.39 (s, 3H).

2.6.2. Preparation of compound 2

BBr_3 (1 ml, 1.47 mmol) was added to the solution of **compound 1** (300 mg, 0.98 mmol) in CH_2Cl_2 (2 ml) at 0 °C under a nitrogen atmosphere. The mixture was allowed to stir at 0 °C for 0.5 h and at room temperature for 3 h. Then the reaction mixture was cooled to 0 °C, and carefully MeOH (100 mL) was added. The solvent was removed in rotary evaporator and the residue was added to MeOH (100 mL). This process was continued three times. The residue was diluted with organic solvent DCM, the precipitate was filtered and washed with DCM to give **compound 2** (160 mg, 56.4%) as a yellow solid, mp >180 °C. MS (LCMS): (m/z, %): 313.2 [(**Compound 2**+H^++Na), 100 %]; Calculated for $C_{19}H_{15}NO_2$: 289.32. ^{1}H NMR (400 MHz, DMSO-d6,): δ (ppm) 10.75 (s, 1H), 9.29 (s, 1H), 7.45 (d, *J* = 8 Hz, 1H), 7.37 (m, 1H), 7.25 (d, *J* = 8.4 Hz, 3H), 7.11 (d, *J* = 8.4 Hz, 2H), 7.07 (d, *J* = 8 Hz, 4H), 6.97 (d, *J* = 8 Hz, 2H).

2.6.3. Preparation of compound TPOD

NH_2OH-HCl (28 mg, 0.40 mmol) and K_2CO_3 (71 mg, 0.51 mmol) were added to the solution of **compound 2** (100 mg, 0.34 mmol) in 5 mL CH_3OH. The mixture was stirred at room temperature over 5 h, then 30 mL water was added and separated four times with 50 mL EtOAc. The organic part was dried over anhydrous Na_2SO_4 and concentrated to dryness in a rotary evaporator under reduced pressure. Finally the residue was refined by column chromatography (Hexane/EtOAc, 1:2, v/v) to yield **TPOD** (60 mg, 58%) as a white solid. mp: 130-140°C, MS

(LCMS): (m/z, %): 327.10 [(**TPOD**+ Na), 100 %]; Calculated for $C_{19}H_{16}N_2O_2$: 304.34. ^{1}H NMR (400 MHz, DMSO-d6), d: 11.01 (s, 1H), 9.36 (s,1H,), 8.20 (s, 1H), 8.06 (s, 1H), 7.54 (m, 1H), 7.35(t, 1H), 7.13 (t, 2H), 7.04 (t, 2H), 6.56 (t, 2H).; 13C NMR (100 MHz, DMSO-d6), δ (ppm) 162.15, 151.55, 146.53, 134.99, 133.62, 129.16, 118.32, 117.12, 115.43.

2.6.4. Preparation of compound TPD

NH_2OH-HCl (30 mg, 0.43 mmol) and K_2CO_3 (75 mg, 0.54 mmol) were added to the solution of **3** (100 mg, 0.36 mmol) in 5 mL CH_3OH. The mixture was stirred at room temperature over 5 h, then 30 mL water was added and separated four times with 50 mL EtOAc. The organic phase was dried over anhydrous Na_2SO_4 and concentrated to dryness in a rotary evaporator under reduced pressure. Finally the residue was refined by column chromatography (Hexane/EtOAc, 1:2, v/v) to yield **TPD** (65 mg, 63%) as a light green solid. mp: 140-150°C, MS (LCMS): (m/z, %): 289.3 [(**TPD**+H^+), 100 %]; Calculated for $C_{19}H_{16}N_2O$: 288.34.

2.6.5. Preparation of compound TPODP complex

In a small round bottomed flask **TPOD** (20 mg, 0.06 mmol) was taken in 2 ml acetonitrile and to this mixture DCP (20.7 mg, 0.06 mmol) was added dropwise. After the completion of the reaction acetonitrile was evaporated in rotary evaporator. To get pure compound purification was done by column chromatography (Hexane: EtOAc = 9:1(v/v)). Finally we got pure product as a light yellow solid. MS (LCMS): (m/z, %): 304.1269 [**TPODP**] + H_2O, 100 %]; Calculated for $C_{19}H_{14}N_2O$: 286.1106. 1H-NMR (CDCl3, 400 MHz): δ (ppm) 8.03 (s, 1H), 7.45(d, J=8.4 Hz, 1H), 7.29 (m, 4H), 7.04 (m, 6H), 6.91 (d, J=8.4 Hz, 2H). 13C-NMR (DMSO-d6, 100 MHz): δ (ppm) 162.14, 151.55, 146.53, 134.99, 133.62, 129.16, 118.32, 117.12, 115.43.

3. Results and discussion

3.1. Synthesis and characterization

Following Vilsmeier-Haack synthesis procedure we first prepared 4 – diphenylamino - 2-methoxy benzaldehyde (Compound1) then demethylation of the Compound1 was carried out using BBr_3 in dichloromethane [56-61]. Finally probe **TPOD** has been synthesized with the reaction of hydroxyl amine in methanol. We confirmed the structural identification of the probe **TPOD** by mass spectroscopy, ^{1}H NMR and ^{13}C NMR (ESI†). We first observed the spectral response of **TPOD** towards DCP in 4:6 v/v CH_3CN–H_2O in HEPES buffer solution. When we added DCP to **TPOD** rapidly ratiometric color change from cyan to green was observed in fluorescence lamp.The reaction is highly dependent on solvent system and the efficient changes was observed at pH 7.4 in CH_3CN–H_2O (4:6 v/v). Thus the probe is applicable to detect DCP under the change in relative humidity.

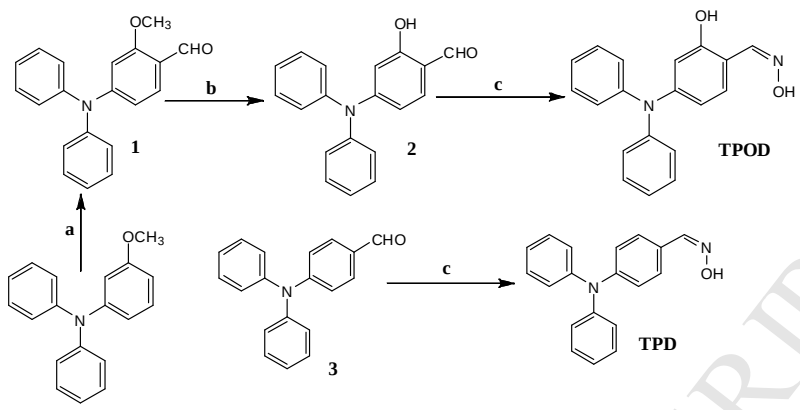

Scheme 1. Reagents and Conditions: (a) DMF, $POCl_3$, Heat 80°C, 6 hrs (b) BBr_3, CH_2Cl_2, r.t, 5 hrs (c) NH_2OH, K_2CO_3,MeOH, r.t, 5 hrs.

3.2. Color and fluorescence response of TPOD towards DCP

Inspection of the absorption spectrum of **TPOD** upon treatment with DCP (Fig.1a) shows that a new band appears at ~405 nm. The band at ~329 nm and ~ 358 nm were gradually decreased and an isosbestic point at ~ 379 nm was appeared. Thus an increase in the long wavelength band and decrease in the short-wavelength band with an isosbestic point at ~379 nm shows that the sensing reaction is a single and promising converted process. The images displayed in inset of Figure 1a showed that the addition of DCP to the aqueous CH_3CN solution of **TPOD** causes a distinct color change from colorless to yellow. Figure 1b shows the change of absorption ratio with successive addition of DCP (0-10 equiv).

As shown in Figure 2a, fluorescence spectra of 1 μM probe **TPOD** solution upon addition of different amount of DCP (0-10 equiv) exhibits a gradual change in the detection mode in a ratiometric way when excited at 379 nm (ϵ_{379} = 11× 10^4 M^{-1} cm^{-1}). Initially it shows a band at ~ 463 nm (ϕ = 0.005) which is gradually decreases and a new peak at ~ 532 nm (ϕ = 0.23) gradually increases with the addition of DCP and saturation came after 10 equiv addition of DCP. The interaction of **TPOD** and DCP was clearly investigated by the appearance of an isoemissive point at ~ 491 nm. In fact the interaction is clearly visible through the color change from cyan to green. Based on the Job's plot (Fig. S17†) it has been proved that the stoichiometry of the formation of compound **TPODP** between probe **TPOD** and DCP is 1:1. The ratio of fluorescence intensities of probe **TPOD** at ~ 463 and ~ 532 nm (I_{463}/ I_{532}) showed a momentous change from 0.782 to 37.05 upon charged with DCP (Fig. 2a), a ~48 fold inflation in the ratiometric emission. Limit of detection (LOD) of **TPOD** towards DCP was calculated (Fig. S15† and S16†) in terms of the formula (3σ/k) and are 0.14 μM and 0.23μM from absorption and fluorescence data through fitting a straight line. Now the plots of fluorescence intensities ratio vs concentration of DCP has been shown in Fig. 2b. In case of our control compound (**TPD**) the change in the spectra (Fig. S13† and S14†) was observed only due to the inhibition of PET from

the oxime-OH as a result of DCP binding. In probe **TPOD** the spectral response is facilitated by the cyclization brought about by the ortho-OH group.

3.3. Interference study of TPOD in presence of active electrophiles

To assess the selectivity of **TPOD** for DCP, we performed the UV-Vis and fluorescence response of **TPOD** to some active electrophiles and nerve agents [62-65], such as thionyl chloride ($SOCl_2$), acetyl chloride (CH_3COCl), phosphorous oxychloride ($POCl_3$), oxalyl chloride $(COCl)_2$, triethyl phosphate (TEP), diisopropyl fluorophosphates (DFP), tributyl phosphate (TBP), diethylcyano phosphonate (DCNP) and dimethylmethyl phosphonate (DMMP). As shown in Figure 3a and 3b, among DCP and these interfering substances, only DCP induced an obvious ratiometric naked eye color change from colorless to yellow and a ratiometric fluorescence change from cyan to green was observed. But the fluorescence of the **TPOD** probe remained undisturbed or was only slightly increased in presence of various interfering agents (Figure S18†). The probe molecule **TPOD** has no response with DCNP and DFP because of having worse leaving aptitude of cyanide and fluoride. Although DCNP, DFP, $SOCl_2$, $POCl_3$ etc can react with the –OH group, but they have no impact on the fluorescence of **TPOD** due to the unique intramolecular cyclization process that is reliant upon the properties of Cl^- as a good leaving group and this sensing event is successful for DCP.

3.4. Time dependent fluorescence investigation

Next we studied response time of **TPOD** at different amount of DCP. We investigated the fluorescence response of **TPOD** over a (0- 1 min) incubation time at the different concentration range of DCP (0- 10 equiv). The fluorescence intensity at ~ 532 nm increases and at ~ 463 nm decreases with increasing concentration of DCP and at higher concentration of DCP promoted the reaction to complete within a min. The change of fluorescence with time graph (Fig. 4a) explored that the reaction of the **TPOD** and DCP could be accomplished within a minute. As expected, with increasing the concentration of DCP the fluorescence intensity at ~532 nm increases and higher concentrations of DCP showed a quick response, and the color and fluorescence changes are easily perceptible to the naked eye and in UV lamp under ~379 nm irradiation. The pseudo-first order rate constant (k_{obs}) calculated for the DCP-prompted cyclization is $k' = 0.149 s^{-1}$ (Fig. 4b). Following the eqn $\ln[(F_{max}-F_t)/F_{max}] = -k't$ [66, 67], Where F_{max} and F_t are the fluorescence intensities at 532 nm at a maximum value acquired after the reaction is terminated and at time t and k' is the observed pseudo-first-order rate constant, the rate constant k' was calculated.

3.5. Computational Studies

To explain optical responses of probe **TPOD** upon reaction with DCP, density functional theory (DFT) and time dependent density functional theory (TDDFT) calculations were performed using the B3LYP/6-31G(d, p) level of Gaussian 09 program [68, 69]. Energy optimized structures molecular orbital of HOMO and LUMO for compound **TPOD** and **TPODP** were

shown in Fig. 5. For **TPOD**, the electron density in the HOMO was diffused over the whole molecule but in LUMO the electron density was mainly accumulated on the oxime group attached phenyl ring. As for **TPODP**, the electron density in HOMO and LUMO orbitals was mostly spread over the benzisoxazole moiety. From Fig. 5 we found that the energy gap for the **TPODP** (3.749 eV) was diminished as compared to the probe **TPOD** (4.074 eV) (Table S3†), indicating the formation of cyclized product.

Now the experimentally observed UV−Vis spectra were compared with the TDDFT of probes **TPOD** and **TPODP**. It is noteworthy that computationally found data to have compatibility with the experimental data. TDDFT calculations showed absorption band at ~348 and ~305 nm corresponds to the electronic transition from HOMO→LUMO (69.81%) (f = 0.6493) and HOMO→LUMO+2 (58.48%) (f = 0.2069) energy states respectively for probe **TPOD** (Table S2†) and absorption band at ~371 and ~402 nm corresponds to the electronic transition from HOMO-1→LUMO+1(61.45%) (f = 0.1076) and HOMO→LUMO (71.68%) (f = 0.3641) energy states respectively for probe **TPODP**. These values are concurrent with the absorbance bands of the two probes **TPOD** and **TPODP** thus the theoretical study supports the experimentally observed absorption bands.

3.6. Reaction path of DCP sensing

To validate the reaction mechanism, when DCP was added to the acetonitrile solution of **TPOD** (procedure is given in experimental section) the oxime hydroxyl group get phosphorylated due to its extreme nucleophilicity and then intramolecular nucleophilic attack from phenolic-OH to the oxime nitrogen leads to the formation of benzisoxazole derivative **TPODP** that has been characterized by HRMS (Fig. S8†) and NMR spectra (Fig. S9†).

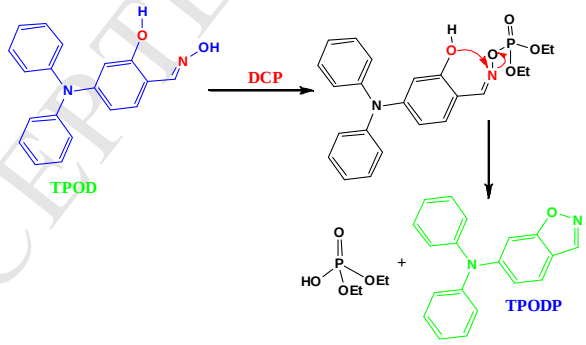

Scheme 2 Plausible reaction mechanism

The structure of **TPODP** and probable mechanism has been shown in Scheme 2. In case of control compound after reaction with DCP, only the oxime hydroxyl get phosphorylated and **TPDP** was formed [70, 71]. The mass spectra of **TPDP** has been given in supporting information**.**

3.7. Recognition of DCP vapor in a sealed vial

We have studied the detection of DCP in gaseous state with probe **TPOD** immersed filter paper. A small slice of filter paper test kit was dipped in a CH_3CN solution contained probe **TPOD** (1 μM) and 10 mM HEPES buffer. Then the probe-loaded filter paper was kept in a sealed vial containing DCP (10 equiv) in CH_3CN solution (Fig. 6). As time proceeded (0-30 sec) in day light filter paper turned from colorless to yellow and in UV lamp cyan color had almost disappeared and green color was appeared. This result implies that our probe **TPOD** may serve as a prospective test kit for on-spot detection of DCP vapour.

3.8. Detection of DCP in soil sample

We explored our probe to confirm the presence of DCP in soil samples. In a beaker 20 μL of DCP was spiked in 6.0 g of soil. Then the spiked soil samples were permitted to stand for 2 hours and separated using chloroform. The chloroform part was evaporate in rotary evaporator and the residual part was dissolved in CH_3CN. Finally the dissolved part was treated with 20 μM **TPOD** solution. Immediately green color was appeared with the spiked sample, while the blank did not give any response (Fig. 7). As Our probe shows ratiometric color change in presence of DCP, so it would not have any practical problem in field trial method.

3.9. Cellular imaging

To further investigate the potential application of **TPOD** for DCP in biological samples, confocal microscopy imaging inside Vero 76 cells (Vero 76, ATCC no. CRL-1587) were performed. Firstly, we have checked the cytotoxicity of probe **TPOD** by MTT assays in Vero 76 cells (Fig. S19†). The result suggesting that low micromolar concentrations of **TPOD** were almost free of toxicity to the Vero 76 cells and thus this sensor is suitable in the cell imaging.

Firstly Vero 76 cells incubated with probe **TPOD** (10 μM) for 20 min at 37 °C in PBS buffer with 0.5%DMSO exhibited blue intracellular fluorescence (Fig. 8B) indicating that **TPOD** is cell permeable. Interestingly when the cells were incubated with 10 μM of **TPOD** for 20 min and further exposed with DCP (40 μM) for another 5min, blue fluorescence was completely replaced with green fluorescence after 5 min (Fig. 8D). Here the bright field images did not show any morphological changes that suggested that Vero 76 cells were viable. These results demonstrate that the probe had effective cellular permeability and possess high resolution in cell imaging. Moreover the ratiometric changes can easily be observed by little changes in DCP levels.

3.10. Single crystal x-ray analysis of TPD

A shinny and X-ray quality single crystal of green colored probe **TPD** was grown by gentle evaporation of solvent from a solution in MeOH–CH_3CN (1:1) at room temperature with ambient condition over few days. The probe crystallizes as monoclinic system with space group

P21/n and CCDC entry no. is 1870349. A summary of the crystallographic parameters and structure refinement details of the probe are given in Table S4†. All calculations were carried out using SHELXL-97 [72,73], ORTEP-32 [74], and PLATON-99 [75] programs. The molecular structure of **TPD** (Fig. 9) is stabilized by a head to tail type cyclic intermolecular hydrogen bonding which is dimeric in nature. In addition to hydrogen bonding, each dimer alternately repeats along b-axis and generates a 1-dimensional supramolecular association (Fig. 10) through a aromatic C− H....π interaction. Each molecule simultaneously participates in ring O—H (donor).....imine - N (acceptor) hydrogen bonding in the oxime part of the molecule forming a chain of centro symmetric rings with single R_2^2 (6) motif. The hydrogen bonding interaction of O1—H1…..N2 with donor -H.....Acceptor distances of 2.799(4) Å to the nearest unit. Supramolecular framework is attained under alternative C−H....π interaction incorporating with the repeating molecule along b-axis (ac plane) and this C− H....π interaction are aromatic in nature with C−H …Cg (2) distance of 2.73(Å).

4. Conclusion

In summary, we have developed a ratiometric fluorescent probe for instant, selective and sensitive detection of DCP vapour. In **TPOD** inhibition of PET process from oxime-hydroxyl to the triphenyl amine moiety and cyclization to the benzisoxazole are responsible for ratiometric color change from cyan to green. We have developed a control compound **TPD** and compared spectral responses with **TPOD**. In the crystal structure of **TPD** we have studied C−H....π and H-bonding interactions. Probe **TPOD** can detect DCP in vapour phase as well as in liquid phase and detection limit of the probe calculated from absorption and fluorescence data are 0.14μM and 0.23μM. Practical observations are well correlated with theoretical calculation by DFT and TDDFT. Furthermore, the probe can be employed to detect trace amounts DCP (10−50 ppm) in soil sample and used in ratiometric fluorescent cellular imaging, which make it an efficient probe for on-site visual detection of environmental DCP gas. We believe that rapidity and selectivity made our present probe highly appealing and multifaceted.

Acknowledgements

We are delighted to acknowledge CSIR-India [Project No. 02(0334)/18/EMR-ll] for financial assistance. SSA would like to give special thanks to UGC-MANF (Student ID: WES-67786), New Delhi for the research grant.

Author Information

[a]Department of Chemistry, Indian Institute of Engineering Science and Technology, Shibpur, Howrah-711103, West Bengal, India, Email: akmahapatra@rediffmail.com, Fax: +913326684564

†Electronic Supplementary Information (ESI) available: [details of any supplementary information available should be included here]. See DOI: 10.1039/b000000x/

Reference

1. Evison D, Hinsley D, Rice P. Chemical weapons. 2002; 324: 332-335.
2. Szinicz L. The Toxicologist and the Response to Incidents with Chemical and Biological Warfare Agents. Toxicology 2005; 214: 167-181.
3. Sidell F R, Borak J. Chemical warfare agents II Nerve agents: Annals of emergency medicine 1992; 21:865-871.
4. Brown K. Up in the air. Science 2004; 305: 1228-1229.
5. Barakat N. H, Zheng X, Gilley C B, MacDonald M, Okolotowicz K, Cashman J R, Vyas S, Beck J M, Hadad C M, Zhang J. Chemical synthesis of two series of nerve agent model compounds and their stereoselective interaction with human acetylcholinesterase and human butyrylcholinesterase. Chemical research in toxicology 2009; 22:1669-1679.
6. Marrs T. C. Organophosphate poisoning. Pharmacology & therapeutics 1993; 58: 51-66.
7. Saladi R, Smith E, Persaud A. Mustard: a potential agent of chemical warfare and terrorism. Clinical and experimental dermatology 2006; 21: 1-5.
8. Shohrati M, Davoudi M, Ghanei M, Peyman M, Peyman A. Cutaneous and ocular late complications of sulfur mustard in Iranian veterans. Cutaneous Ocul Toxicol 2007; 26: 73-81.
9. Kehe K, Szinicz L. Medical aspects of sulphur mustard poisoning. Toxicology 2005; 214: 198-209.
10. Kumar V, Anslyn E. V. A Selective Turn-On Fluorescent Sensor for Sulfur Mustard Simulants, J Am Chem Soc 2013; 135: 6338-6344.
11. Davis K. G, Aspera G. Exposure to liquid sulfur mustard. Ann Emerg Med 2001; 37: 653-656.
12. Pathak U, Raza S. K, Kulkarni A S, Vijaaraghvan R, Kumar P, Jaiswal D K. Novel S-Substituted Aminoalkylamino Ethanethiols as Potential Antidotes against Sulfur Mustard Toxicity. J Med Chem 2004; 47: 3817-3822.
13. Dale T J, Rebek J, Fluorescent Sensors for Organophosphorus Nerve Agent Mimics. J Am Chem Soc 2006; 128: 4500-4501.
14. Greñu B D, Moreno D, Torroba T, Berg A, Gunnars J, Nilsson T, Nyman R, Persson M, Pettersson J, Eklind I, Wasterby P. Fluorescent Discrimination between Traces of Chemical Warfare Agents and Their Mimics. J Am Chem Soc 2014; 136: 4125-4128.
15. Kim H J, Lee J H, Lee H, Lee J H, Lee J H, Jung J H, Kim J S. A mesoporous, silica-immobilized-nanoparticle colorimetric chemosensor for the detection of nerve agents. Adv Funct Mater 2011; 21: 4035-4040.
16. Lee J, Seo S, Kim J. Colorimetric Detection of Warfare Gases by Polydiacetylenes Toward Equipment-Free Detection. Adv Funct Mater 2012; 22: 1632-1638.
17. Rochat S B, Swager T M. Water-Soluble Cationic Conjugated Polymers: Response to Electron-Rich Bioanalytes. J Am Chem Soc 2013; 135: 17703-17706.
18. Zhang S W, Swager T M. Fluorescent Detection of Chemical Warfare Agents: Functional Group Specific Ratiometric Chemosensors. J Am Chem Soc 2003; 125: 3420-3421.

19. Royo S, Martı´nez-Ma´nez R, Sanceno´n F, Costero A M, Parrab M, Gil S. Chromogenic and fluorogenic reagents for chemical warfare nerve agents' detection. Chem Commun 2007; 0: 4839-4847.
20. Burnworth M, Rowan S J, Weder C. Fluorescent sensors for the detection of chemical warfare agents. Chem Eur J 2007; 13: 7828.-7836.
21. Diehl K L, Anslyn E V. Array sensing using optical methods for detection of chemical and biological hazards. Chem Soc Rev 2013; 42: 8596-8611.
22. Zhou X, Zeng Y, Liyan C, Wu X, Yoon J. A Fluorescent Sensor for Dual-Channel Discrimination between Phosgene and a Nerve-Gas Mimic. Angew Chem Int Ed 2016; 55: 4729-4733.
23. So H S, Angupillai S, Son Y A. Prompt liquid-phase visual detection and low-cost vapor-phase detection of DCP: a chemical warfare agent mimic. Sens Actuators B 2016; 235: 447-456.
24. Hewage H S, Wallace K J, Anslyn E V. Novel chemiluminescent detection of chemical warfare stimulant. Chem Commun 2007; 0: 3909-3911.
25. Han S, Xue Z, Wang Z, Wen T B. Visual and fluorogenic detection of a nerve agent simulant via a Lossen rearrangement of rhodamine–hydroxamate. Chem Commun 2010; 46: 8413-8415.
26. Louise-Leriche L, Paunescu E, Saint-Andre G, Baati R, Romieu A, Wagner A, Renard P Y. A HTS assay for the detection of organophosphorus nerve agent scavengers. Chem Eur J 2010; 16: 3510-3523.
27. Zheng X, Okolotowicz K, Wang B, Macdonald M, Cashman J R, Zhang J. Direct detection of the hydrolysis of nerve agent model compounds using a fluorescent probe. Chem Biol Interact 2010; 187: 330-334.
28. Gotor R, Royo S, Costero A M, Parra M, Gil S, Martı´nez-Ma´n˜ez R, Sanceno´n F. Nerve agent simulant detection by using chromogenic triaryl methane cation probes. Tetrahedron 2012; 68: 8612-8616.
29. Barba-Bon A, Costero A M, Gil S, Harriman A, Sancenon F. Highly Selective Detection of Nerve-Agent Simulants with BODIPY Dyes. Chem Eur J 2014; 20: 6339-6347.
30. Sayed S El, Pascual L, Agostini A, Martinez-Manez R, Sancenon F, Costero A M, Parra M, Gil S. A Chromogenic Probe for the Selective Recognition of Sarin and Soman Mimic DFP. Chemistry Open 2014; 3: 142-145.
31. Dale T J, Rebe Jr J. Hydroxy oximes as organophosphorus nerve agent sensors. Angew Chem Int Ed 2009; 48: 7850-7852.
32. Wu X, Wu Z, Han S. Chromogenic and fluorogenic detection of a nerve agent simulant with a rhodamine-deoxylactam based sensor. Chem Commun 2011; 47: 11468-11470.
33. Balamurugan A, Lee H. A Visible Light Responsive On–Off Polymeric Photoswitch for the Colorimetric Detection of Nerve Agent Mimics in Solution and in the Vapor Phase, Macromolecules 2016; 49: 2568-2574.
34. Jang Y J, Mulay S V, Kim Y, Jorayev P, Churchill D G. Nerve agent simulant diethyl chlorophosphate detection using a cyclization reaction approach with high stokes shift system. New J Chem 2017; 41: 1653-1658.

35. Lei Z, Yang Y. A Concise Colorimetric and Fluorimetric Probe for Sarin Related Threats Designed via the "Covalent-Assembly" Approach. J Am Chem Soc 2014; 136: 6954-6997.
36. Mahapatra A K, Maiti K, Manna S K, Maji R, Mondal S, Mukhopadhyay C D, Sahoo P, Mandal D. A cyclization-induced emission enhancement (CIEE)-based ratiometric fluorogenic and chromogenic probe for the facile detection of a nerve agent simulant DCP. Chem Commun 2015; 51: 9729-9732.
37. Wallace K J, Fagbemi R I, Folmer-Andersen F J, Morey J, Lynth V M, Anslyn E V. Detection of chemical warfare simulants by phosphorylation of a coumarin oximate. Chem Commun 2006; 37: 3886-3888.
38. Ren Y, Yamataka H. The α-Effect in Gas-Phase SN^2 Reactions: Existence and the Origin of the Effect. J Org Chem 2007;72: 5660-5667.
39. Klopman G, Tsuda K, Louis J B, Davis R E. Supernucleophiles-I: The alpha effect. Tetrahedron 1970; 26: 4549-4554.
40. Edwards J O, Pearson R G. The Factors Determining Nucleophilic Reactivities. J Am Chem Soc 1962; 84: 16-24.
41. Jencks W P, Carriuolo J. Reactivity of Nucleophilic Reagents toward Esters. J Am Chem Soc 1960; 82: 1778-1786.
42. Terrier F, Rodriguez-Dafonte P, Le Guevel E, Moutiers G. Revisiting the reactivity of oximate α-nucleophiles with electrophilic phosphorus centers. Relevance to detoxification of sarin, soman and DFP under mild conditions. Org Biomol Chem 2006; 4: 4352-4363.
43. Valeur B, Santos M N B. Molecular Fluorescence Principles and Applications 2013; 2: 77-78.
44. Climent E, Biyikal M, Gawlitza K, Dropa T, Urban M, Costero A M, Máñez R M, Rurack K. A Rapid and Sensitive Strip-Based Quick Test for Nerve Agents Tabun, Sarin and Soman Using BODIPY-Modified Silica Materials. Chem Eur J 2016; 22: 11138-11142.
45. Wrobel A T, Johnstone T C, Liang A D, Lippard S J, Fuentes P R. A Fast and Selective Near-Infrared Fluorescent Sensor for Multicolor Imaging of Biological Nitroxyl (HNO). J Am Chem Soc 2014; 136: 4697-4705.
46. Walton I, Davis M, Munro L, Catalano V J, Cragg P J, Huggins M T, Wallace K J. A fluorescent dipyrrinone oxime for the detection of pesticides and other organophosphates. Org Lett 2012; 14: 2686-2689.
47. Ali S S, Gangopadhyay A, Maiti K, Mondal S, Pramanik A K, Guria U N, Uddin Md R, Mandal S, Mandal D, Mahapatra A K. A chromogenic and ratiometric fluorogenic probe for rapid detection of a nerve agent simulant DCP based on a hybrid hydroxynaphthalene–hemicyanine dye. Org Biomol Chem 2017; 15: 5959-5967.
48. Sidell F R, Borak J. Chemical warfare agents: II. Nerve agents. Ann. Emerg Med 1992; 21: 865-871.
49. Yang Y C. Acc Chemical Detoxification of Nerve Agent VX. Chem Res 1999; 32: 109-115.

50. Sohn H, Létant S, Sailor M J, Trogler W C. Detection of Fluorophosphonate Chemical Warfare Agents by Catalytic Hydrolysis with a Porous Silicon Interferometer. J Am Chem Soc 2000; 122: 5399-5400.
51. Somani S, Solana R, Dube S. Chemical Warfare Agents: Academic Press: San Diego. CA 1992; 67-123.
52. Sambrook M, Notman S. Supramolecular chemistry and chemical warfare agents: from fundamentals of recognition to catalysis and sensing. Chem Soc Rev 2013; 42: 9251-9267.
53. Ali S S, Gangopadhyay A, Pramanik A K, Samanta S K, Guria U N, Manna S, Mahapatra A K. Real time detection of the nerve agent simulant diethylchlorophosphate by nonfluorophoric small molecules generating a cyclization-induced fluorogenic response. Analyst 2018; 143: 4171-4179.
54. Kim K, Tsay O G. Atwood, D. A, Churchill, D. G. Destruction and detection of chemical warfare agents. Chem. Rev 2011; 111: 5345-5403.
55. Hu X X, Su Y T, Ma Y W, Zhan X Q, Zheng H, Jiang Y B. A near infrared colorimetric and fluorometric probe for organophosphorus nerve agent mimics by intramolecular amidation. Chem Commun 2015; 51: 15118-11521.
56. Marson C M. For an excellent review on the Vilsmeier-Haack reaction of carbonyl compounds. Tetrahedron 1992; 48: 3659-3726.
57. Black R M, Clarke R J, Read R W, Reid M T. Application of gas chromatography-mass spectrometry and gas chromatography-tandem mass spectrometry to the analysis of chemical warfare samples found to contain residues of the nerve agent sarin, sulphur mustard and their degradation products. J Chromatogr A 1994; 662: 302-321.
58. Steiner W E, Klopsch S J, English W A, Clowers B H, Hill H H. Detection of a Chemical Warfare Agent Simulant in Various Aerosol Matrixes by Ion Mobility Time-of-Flight Mass Spectrometry. Anal Chem 2005; 77: 4792-4799.
59. Khan M A K, Long Y T, Schatte G, Kraatz H B. Surface Studies of Aminoferrocene Derivatives on Gold: Electrochemical Sensors for Chemical Warfare Agents. Anal Chem 2007; 79: 2877-2882.
60. Liu G, Lin T. Electrochemical stripping analysis of organophosphate pesticides and nerve agents. Electrochem Commun 2005; 7: 339-343.
61. Liu G, Lin Y. Biosensor Based on Self-Assembling Acetylcholinesterase on Carbon Nanotubes for Flow Injection/Amperometric Detection of Organophosphate Pesticides and Nerve Agents. Anal Chem 2006; 78: 835-843.
62. Russell A J, Berberich J A, Drevon G F, Koepsel R R. Biomaterials for Mediation of Chemical and Biological Warfare Agents. Annu Rev Biomed. Eng 2003; 5: 1-27.
63. Wang J, Timchalk C, Lin Y. Carbon Nanotube-Based Electrochemical Sensor for Assay of Salivary Cholinesterase Enzyme Activity: An Exposure Biomarker of Organophosphate Pesticides and Nerve Agents. Environ Sci Technol 2008; 42: 2688-2693.

64. Jo J, Lee D. Turn-On Fluorescence Detection of Cyanide in Water: Activation of Latent Fluorophores through Remote Hydrogen Bonds That Mimic Peptide β-Turn Moti. J Am Chem Soc 2009; 131: 16283-16291.
65. Chen L, Wu D, Yoon J. Recent Advances in the Development of Chromophore-Based Chemosensors for Nerve Agents and Phosgene. ACS Sens 2018; 3: 27-43.
66. Wu W H, Dong J J, Wang X, Li J, Sui S H, Chen G Y, Liu J W, Zhang M. Fluorogenic and chromogenic probe for rapid detection of a nerve agent simulant DCP. Analyst 2012; 137: 3224-3246.
67. Vishnuvardhan V, Kalyan Y, Prathish K P, Gangadhar B, Tharakeswar Y, Rao T P, Naidu G R. Imprinted Polymer Inclusion Membrane Based Potentiometric Sensor for Determination and Quantification of Diethyl Chlorophosphate in Natural Waters. Am J Anal Chem 2011; 2: 376-382.
68. Portal D S, Ordejon P, Artacho E, Soler J M. Density-functional method for very large systems with LCAO basis sets. International Journal of Quantum Chemistry 1997; 65: 453-461.
69. Kresse G, Furthmuller J. Efficiency of ab-initio total energy calculations for metals and semiconductors using a plane-wave basis set. Computational Materials Science 1996; 6: 15-50.
70. Lee H, Kim H J, Novel fluorescent probe for the selective detection of organophosphorous nerve agents through a cascade reaction from oxime to nitrile via isoxazole. Tetrahedron 2014; 70: 2966-2970.
71. Radic Z, Dale T, Kovarik Z, Berend S, Garcia E, Zhang L, Amitai G, Green C, Radic B, Duggan B M, Ajami D, Rebek J, Taylor P. Catalytic detoxification of nerve agent and pesticide organophosphates by butyrylcholinesterase assisted with non-pyridinium oximes. Biochem J 2013; 450: 231-242.
72. Sheldrick G M. SHELXS-97. Program for the Solution of Crystal Structure: University of Gottingen. Germany 1997.
73. Sheldrick G M. SHELXL-97. Program for the Refinement of Crystal Structure: University of Gottingen. Germany1997.
74. Farrugia L J. ORTEP-3 for windows- a version of ORTEP-III with a Graphical User Interface (GUI). J Appl Cryst 1997; 30: 565.
75. Spek A L. PLATON: Molecular Geometry Program. University of Utrecht, The Netherlands 1999.

Figure Captions

Fig. 1 (a) Absorption spectra of **TPOD** (1μM) in $CH_3CN–H_2O$ (4:6 v/v) in presence of DCP (40 μM) and 10 mM HEPES buffer, pH 7.4, at 25^oC. (b) Plot of absorption ratio change and concentration of DCP.

Fig. 2 (a) Fluorescence spectra of **TPOD** (1μM) in $CH_3CN–H_2O$ (4:6 v/v) in presence of DCP (40 μM) and 10 mM HEPES buffer, pH 7.4, at 25^oC, λex = 379 nm. (b) Plot of fluorescence ratio change and concentration of DCP.

Fig. 3 (a) Relative absorption spectra of **TPOD** (1μM) in CH_3CN-H_2O (4:6 v/v, 10 mM HEPES buffer, pH 7.4 at 25 ^oC) in presence of DCP (10 equiv) and 50 equiv of CH_3COCl, $SOCl_2$, $POCl_3$, $(COCl)_2$, TEP, DFP, TBP, DCNP and DMMP. (b) Relative fluorescence spectra of of **TPOD** (1μM) in CH_3CN-H_2O (4:6 v/v, 10 mM HEPES buffer, , pH 7.4 at 25 ^oC) in presence of DCP (10 equiv) and 50 equiv of CH_3COCl, $SOCl_2$, $POCl_3$,$(COCl)_2$, TEP, DFP, TBP, DCNP and DMMP.

Fig.4 (a) Time dependent fluorescence enhancement of **TPOD** (1 μM) with increasing concentration of DCP (0- 10 equiv) in CH_3CN-H_2O (10 mM HEPES buffer, 4:6 v/v, pH 7.4 at 25^oC) solution, λex = 379 nm; λem = 532 nm. (b) Pseudo first order rate constant plot of **TPOD** (1 μM) in presence of DCP (40 μM).

Fig.5 Energy minimized structure and HOMO-LUMO energy gap of **TPOD** and **TPODP.**

Fig.6 Photograph of color and fluorescence response of **TPOD** upon exposure to DCP (0-10 equiv) for 0-30 sec. Photographs were taken in day light and in UV-lamp.

Fig.7 Fluorescence spectra of free **TPOD**, Unspiked sample and Spiked sample.

Fig.8 Confocal microscopy imaging of **TPOD** in Vero 76 cells (Vero 76, ATCC no. CRL-1587): (A) Bright field image of the cells stained with probe **TPOD** at 1.0×10^{-6} M, (B) Image scan of the probe **TPOD** at 1.0×10^{-6} M concentration for 20 min at 37 ^oC, (C) Merged images of B and A, (D) Bright field image of the cells treated with **TPOD** at 1.0×10^{-6} M and DCP at concentration 4.0×10^{-5} M, (E) Image scan of the cells treated with probe **TPOD** at 1.0×10^{-6} M for 20 min and further incubated with DCP at concentration 4.0×10^{-5} M for 5 min; and green fluorescence signal was detected. (F) Merged images of D and E. λ_{ex}= 379 nm, λ_{em}= 460- 540 nm. Scale bar, 100 μm.

Fig.9 Ortep diagram of **TPD**, showing 35% thermal ellipsoids probability level for non-H atoms with atom numbering scheme.

Fig.10 The crystal packing diagram of **TPD** shows head to tail O-H…N hydrogen bonded cyclic dimmer and each dimer constitutes a 1-D supramolecular network involving C− H....π interaction viewed along the b-axis (H atoms not involved are omitted in for clarity).

Fig. 1

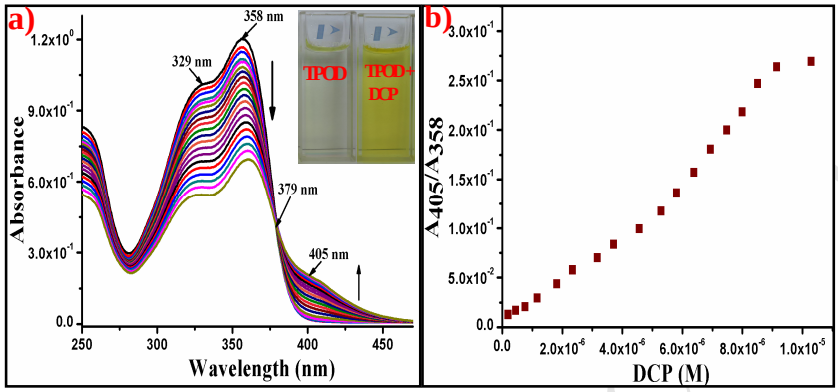

Fig. 2

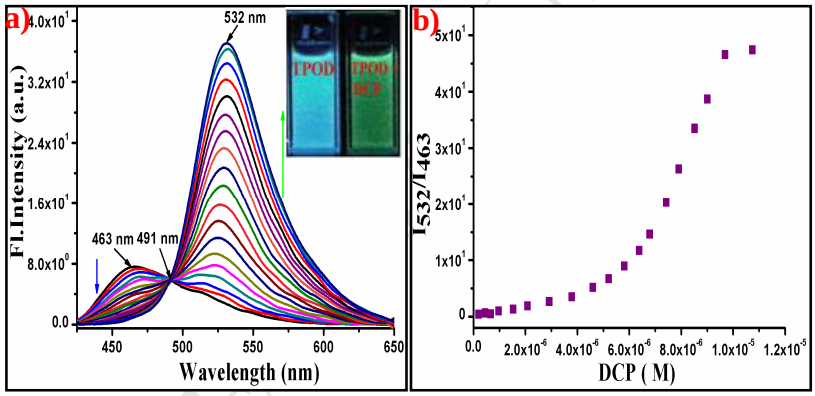

Fig. 3

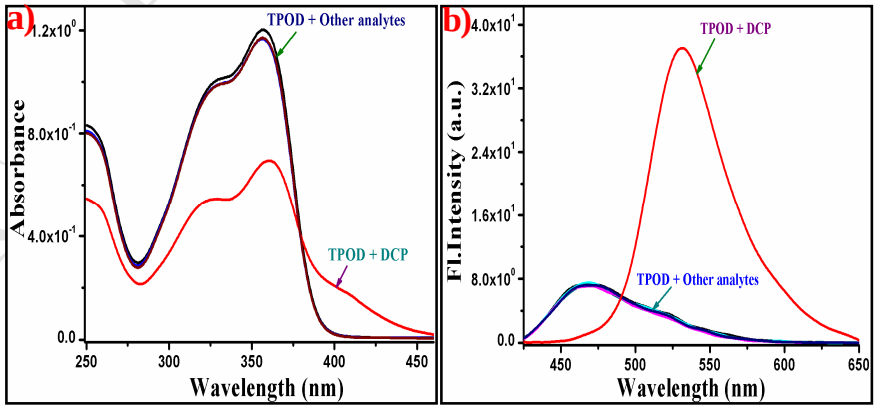

Fig. 4

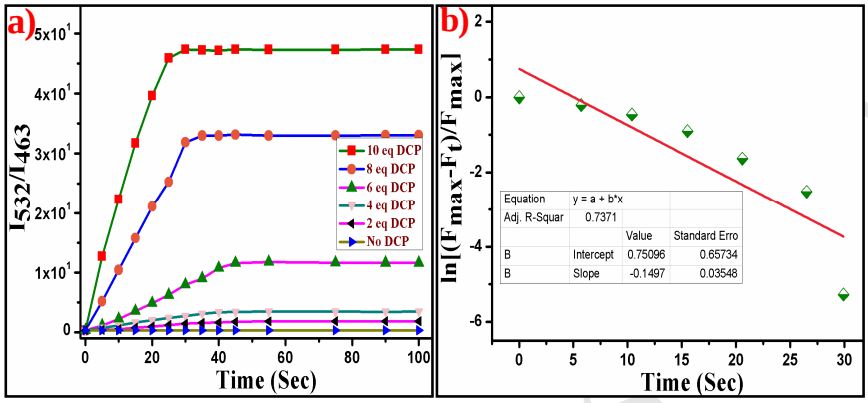
a)
I_{532}/I_{463}
Time (Sec)
10 eq DCP
8 eq DCP
6 eq DCP
4 eq DCP
2 eq DCP
No DCP
b)
$\ln[(F_{max}-F_t)/F_{max}]$
Time (Sec)
Equation y = a + b*x
Adj. R-Squar 0.7371
Value Standard Erro
B Intercept 0.75096 0.65734
B Slope -0.1497 0.03548

Fig. 5

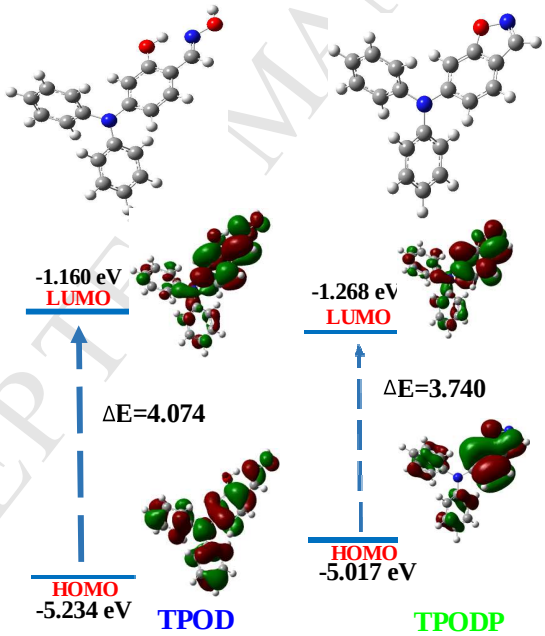
-1.160 eV
LUMO
ΔE=4.074
HOMO
-5.234 eV
TPOD
-1.268 eV
LUMO
ΔE=3.740
HOMO
-5.017 eV
TPODP

Fig. 6

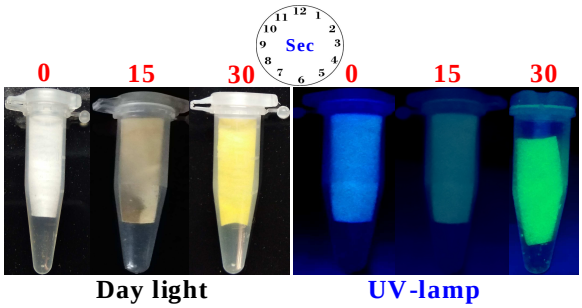

Fig. 7

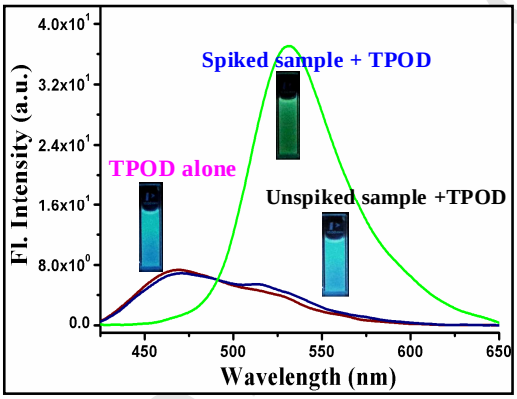

Fig. 8

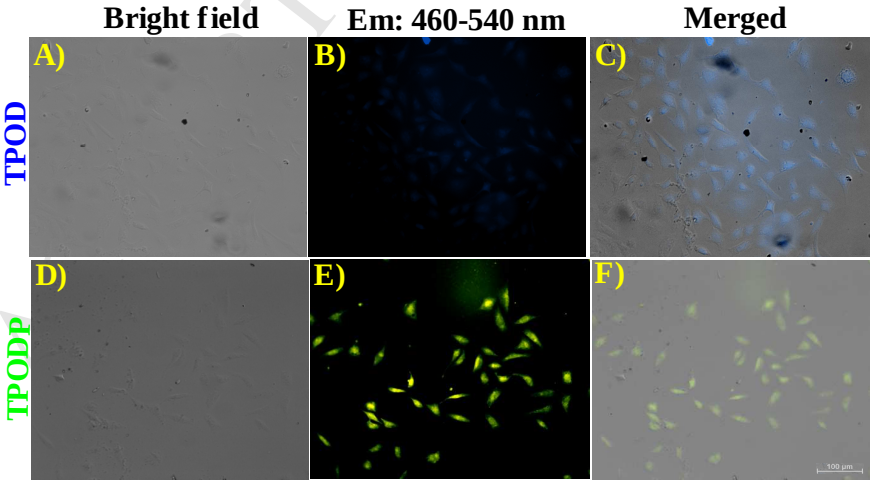

Fig. 9

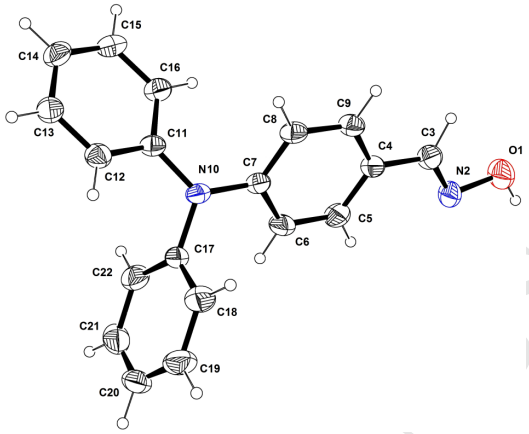
C15
C14
C16
C13
C11
C12
N10
C7
C8
C9
C4
C3
N2
O1
C5
C6
C17
C22
C18
C21
C19
C20

Fig. 10

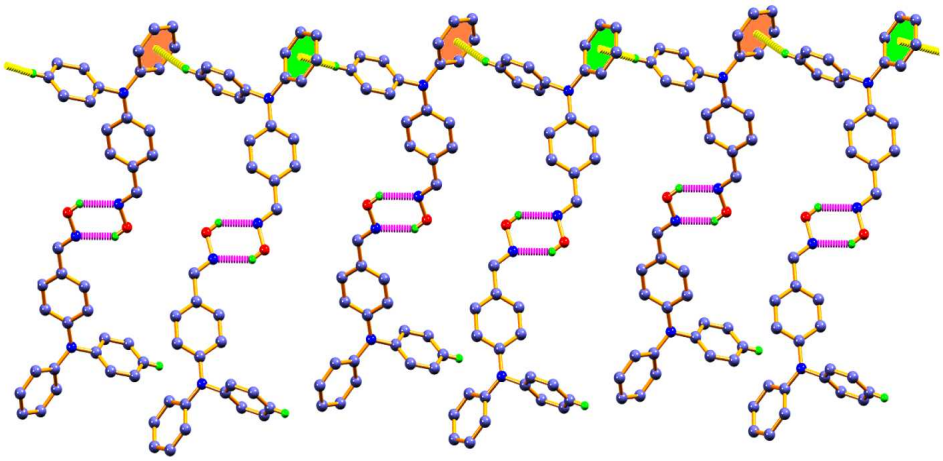

Ratiometric sensing of nerve agent mimic DCP through in situ Benzisoxazole formation

Syed Samim Ali, [a] Ankita Gangopadhyay, [a] Ajoy Kumar Pramanik,[a] Uday Narayan Guria,[a] Sandip Kumar Samanta [a] and Ajit Kumar Mahapatra[*a]

[a]Department of Chemistry, Indian Institute of Engineering Science and Technology, Shibpur, Howrah – 711103, India.

*****Corresponding author: Tel.: +91 33 2668 4561; fax: +91 33 26684564;

E-mail: mahapatra574@gmail.com, akmahapatra@rediffmail.com

Highlights

1. 4-diphenylamino-2-hydroxy benzaldehyde oxime has been synthesized for the ratiometric detection of DCP.

2. Ratiometric color and fluorescence change were achieved due to cyclization and PET mechanism.

3. The probe **TPOD** can be utilised in-field detection of DCP by using a portable filter paper strip.

4. Probe **TPOD** has an exceptional selectivity towards DCP over other nerve agents and active electrophiles.

5. The probe **TPOD** can able to detect DCP in soil sample and biological sample also.

6. Significance of ortho hydroxyl group in **TPOD** could be justified by comparing with a probe **(TPD)** which does not contain that functionality.